Characterisation of copper mechanical properties using I-kaz 4D analysis method via piezofilm sensor

Mohd Irman Ramli[1,*], Mohd Zaki Nuawi[2], Nor Azazi Ngatiman[1], Mudather Bahr Eldeen Hamid Nour[2], Muhammed Noor Hashim[1], Ahmad Fuad Ab. Ghani[1]

[1)] Faculty of Engineering Technology, Universiti Teknikal Malaysia Melaka, Hang Tuah Jaya, 76100 Durian Tunggal, Melaka, Malaysia.
[2)] Department of Mechanical and Materials Engineering, Faculty of Engineering and Built Environment, Universiti Kebangsaan Malaysia, 43600 Bangi, Selangor, Malaysia.

[*]Corresponding e-mail: irman@utem.edu.my

Keywords: I-kaz 4D; impact hammer; piezofilm sensors

ABSTRACT – An alternative advanced statistical analysis method known as the I-kaz 4D or I-kaz 4 channels which using the sensor fusion concept by applying four sensors to collect the vibration signals that excited by the impact hammer was introduced in this study. The study carried for copper (Cu). The specimens were in shape of circular, rectangular and square. The impact force were set with the range of different forces. The four piezofilm sensors been placed at specimen's surface to observe and record the vibration signal after the impact. The obtained results been compared with the results obtained by I-kaz 4D method.

1. INTRODUCTION

The present study deals with the use of the impact testing method to produce an excitation within the metallic material specimen. This method is relatively a simple technique to implement at the same time there is challenges in obtaining symmetric results. The most important features of present method are that it does not require a complex and expensive machines instead it just needs some hardware, which make this technique very attractive and convenience. The implementation process consists of the impact hammer, analyser and software. A piezoelectric sensor is used to monitor the vibration signal of the specimen under the impulse excitation in order to analyse and determine its characteristic frequencies [1]. Further analysis is done on the vibration signals observed during the test impact and the possible correlation between these signals and the specific material properties were studied by digital signal analysis approach using the I-kaz 4D.

2. METHODOLOGY

The characterization of material properties in this study is based on the analysis of vibration signal resulting from the impact force from the impact hammer [2]. With the help of Labview software 2015, DAQ NI 9234 National Instrument data collection system, and Rion-Note multi-factional measuring system platform SA-A1 device, data input from impact hammer were being processed, stored and analyzed. Two types of signals were observed by the developed softwares, i.e., the vibration signal from the piezofilm sensor and the impact force signal. Observations were carried out using appropriate equipment to measure the signals of different type. Next, an alternative methods for signal analysis and interpreting signals were used. Figure 1 shows the schematic diagram of the experiment while Table 1 shows the experiment components.

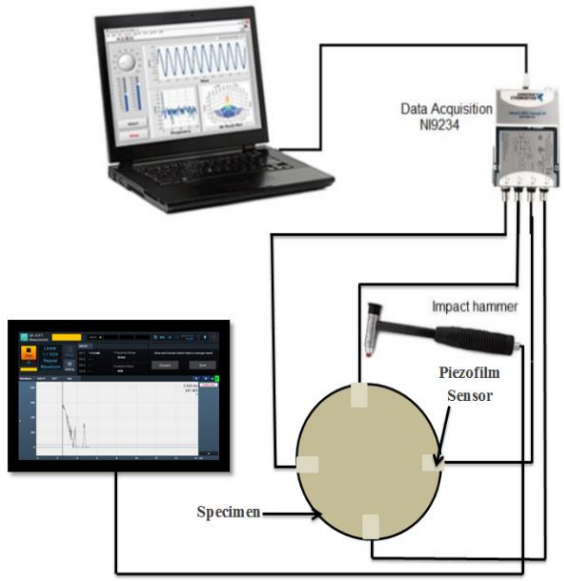

Figure 1 Schematic diagram of the experiment.

Table 1 Experiment components.

Component	Specifications	Quantity
Impact hammer	D15 cm	1
The data acquisition device	NI 9234 (four-channel)	1
Signal Express software	Multichannel High speed	1
Rion SA-A1 device software	Multi-factional measuring system	1
Piezofilm sensor	SDT1- molded plastic	1
Specimen	Copper(Cu)	3
Supporter	polyurethane foam	3

I-kaz 4D is using the direct fusion where the data are collected from 4 homogeneous sensors. The formula of I-kaz 4D is as follows:

$$Z_{4D}^{\infty} = \frac{1}{n}\sqrt{k_1 s_1^4 + k_2 s_2^4 + k_3 s_3^4 + k_4 s_4^4} \quad (1)$$

Where:

Z_{4D}^{∞} : I-kaz 4D cofficient
n : number of samples
k : kurtosis
s : standard deviation.

3. RESULTS AND DISCUSSION

3.1 Type of signals

Two types of signal data measured in the experiment simultaneously, namely the signal of the impact force and vibration signal captured by the four piezofilm sensors for each of the circular, rectangular and square shapes which will be analyzed using I-kaz 4D, beside the vibration signal captured by only one piezofilm sensor for the circular shape specimen which will be analyzed using FFT method. The two signals are generated during the process of impact between the impact hammer and the material specimens [3]. Figure 2 show the vibration signal of copper.

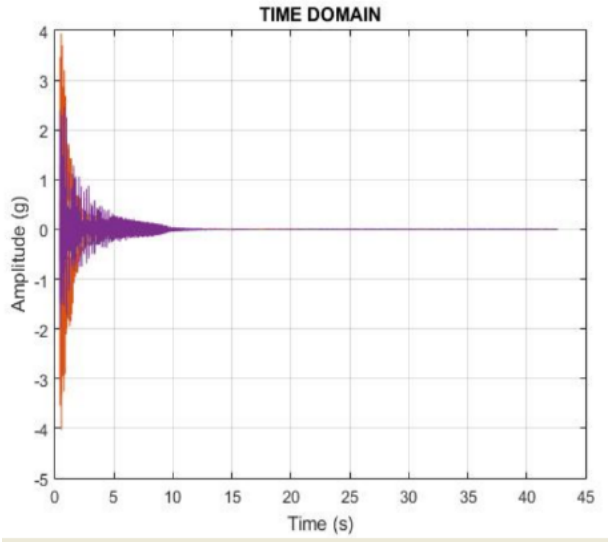

Figure 2 Vibration signal of circular copper at 300 N.

The vibration signals obtained from the impulse excitation experiment were analysed using the new developed statistical methods known as I-kaz 4D. The I-kaz 4D method known as Integrated kurtosis-based algorithm using four sensors simultaneously to record the vibration signals.

In this method, the time domain of vibration signals that captured by the piezofilm sensors were analysed to extract the information contained in the signal content. The statistical analysis of I-kaz methods is based on the concept of scattering data to a central value [4].

3.2 Correlation between piezofilm signals and copper mechanical properties

To study the existence of correlation between the vibration signal and any of mechanical properties of the metal materials of the three different shapes that used in the experiment, the vibration signal that recorded by the piezofilm sensor has been analysed by applying the I-kaz 4D statistical analysis method which produced the I-kaz 4D coefficient.

The pattern of changing in the magnitude of these I-kaz 4D coefficients with respect to the changing of the impact force that applied on the specimen for all shapes has been studied by plotting the I-kaz 4D coefficients of the piezofilm sensors. Figure 3 shows the graph obtained and Table 2 shows the data.

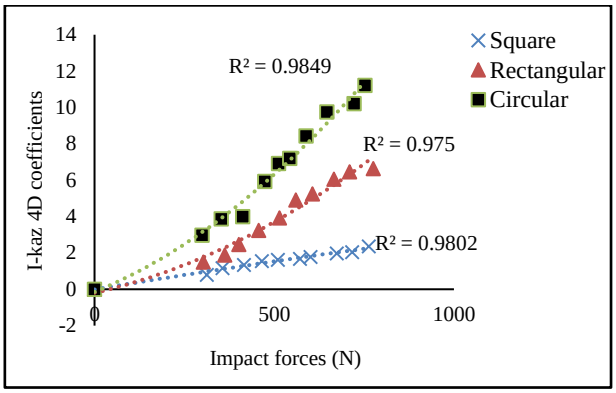

Figure 3 I-kaz 4D vs impact forces.

Table 2 Quadratic equations and coefficients (R^2) of copper.

Shape	Linear equations	(R^2)
Circular	$y = 9.872 \times 10^{-12} x^2 + 8.1236 \times 10^{-9} x - 1.2412 \times 10^{-7}$	0.985
Square	$y = 3.029 \times 10^{-8} x + 3.963 \times 10^{-7}$	0.980
Rectangular	$y = 7.498 \times 10^{-12} x^2 + 4.202 \times 10^{-9} x - 1.737 \times 10^{-7}$	0.975

4. CONCLUSION

In this study, methods of characterisation of the material properties using advance statistical analysis of vibration signal known as I-kaz 4D has been developed. Also, the dynamic response technique was used to compare it's result with the result obtained when I-kaz 4D technique were used, where I-kaz method showed a significant better result.

ACKNOWLEDGEMENT

This project is supported by Universiti Teknikal Malaysia Melaka, UTeM (grant no.: PJP/2018/FTK(5B)/S01596).

REFERENCES

[1] Bruno, L., Felice, G., Pagnotta, L., Poggiliani, A. & Stigliano, G. (2008). Elastic characterisation of plates of any shape via static testing. *International Journal of Solids and Structure*, *45*(3-4), 908-920.

[2] Karim, Z., Izatul, H.A.R., Azuan, S.A.S., Mastura, S., Said, A.Y.M., Bahari, A.R., Ghani, J.A. & Nuawi, M.Z. (2013). Material mechanical property correlation study using vibration signal analysis. *Australian Journal of Basic and Applied Sciences*, *7*(4), 94-99.

[3] Ramli, M.I., Nuawi, M.Z., Abdullah, S., Rasani, M.R.M., Ahmad, M.A.F. & Seng, K.K. (2017). An

investigation on light structure modal parameter by using experimental modal analysis method via piezofilm sensor. *Jurnal Teknologi*, *79*(6), 159-165.

[4] Ziyad, S.S., Nuawi, M.Z., Jasim, M.T., Bahari, A.R. & Nadia, F.M. (2015). Characterisation of polymer material using I-kaz^{TM} analysis method under impact hammer excitation technique. *Journal of Applied Sciences*, *15*(1), 138-145.

Training feedforward neural networks for fault diagnosis of ball bearing

Tuan A.Z. Rahman[1,*], A. As'arry[1], N.A. Abdul Jalil[1], Raja Kamil[2]

[1)] Sound and Vibration Research Group, Department of Mechanical and Manufacturing Engineering, Faculty of Engineering, Universiti Putra Malaysia (UPM), 43400 Serdang, Selangor, Malaysia.
[2)] Department of Electrical and Electronic Engineering, Faculty of Engineering, Universiti Putra Malaysia, 43400 Serdang, Selangor, Malaysia.

[*]Corresponding e-mail: tuanzahidi@upm.edu.my

Keywords: Artificial neural networks; damage classification; stochastic fractal search

ABSTRACT – Vibration-based condition monitoring plays important roles for early fault detection and diagnosis of expensive rotating machinery. This paper presents the application of a novel metaheuristic approach named chaos-enhanced stochastic fractal search (CFS) to train feedforward neural networks (FNNs) for monitoring a ball bearings system. The vibration response data are analyzed using statistical methods to characterize several defects of ball bearings and generate vibration signature features. Then, a novel CFS-based FNNs approach is applied to classify these ball bearings conditions. The results show that the proposed approach produces comparable classification accuracy as parameters of the FNNs were optimized systematically using CFS algorithm.

1. INTRODUCTION

The bearings are the most important mechanical elements of rotating machinery. The major source of most mechanical faults in rotating machinery is the bearing fault [1]. Therefore, early bearing faults diagnosis and monitoring have become pivotal to avoid the production losses and improve the safety and availability of the machinery [2]. Many faults diagnosis approaches have been proposed over the years. Vibration signals generated by the faults have proved to be a powerful diagnostic technique [3]. With the advancement of evolutionary algorithms (EAs), the accuracy of the proposed diagnostic techniques can be improved in terms of searching for the appropriate parameters and features selection [4]. In this study, a metaheuristic algorithm named Stochastic Fractal Search (SFS) algorithm is applied to train a feedforward neural networks (FNNs) for ball bearings faults diagnosis [5].

2. METHODOLOGY

Over the years, the Case Western Reserve University (CWRU) Bearing Data Center has become a standard reference in the bearing diagnostics field and widely used [6]. Figure 1 shows the schematic diagram of experimental setup of the CWRU bearing. Experiments were conducted using a 2 HP Reliance Electric Motor, and acceleration data was measured at locations near to and remote from the motor bearings. Motor bearings were seeded with faults using electro-discharge machining.

Figure 2 shows the acceleration data of different fault types and sizes. Each data were plotted within the same range of [-6 6] ms^{-2}. Three faults which are ball (B) fault (left), inner race (IR) fault (middle) and outer race (OR) fault (right) were introduced to the drive end bearing. The defects sizes are 0.007 inches (first row) and 0.021 inches (second row). Each original signal was divided into 100 signals for each condition of fault types and sizes. Four features based on two time-domain and two frequency-domain were calculated which are mean and standard deviation of data points/spectrum lines.

The feedforward neural networks (FNNs) with two layers are the most popular neural networks in practical applications and suitable for classification of nonlinearly separable patterns [7].

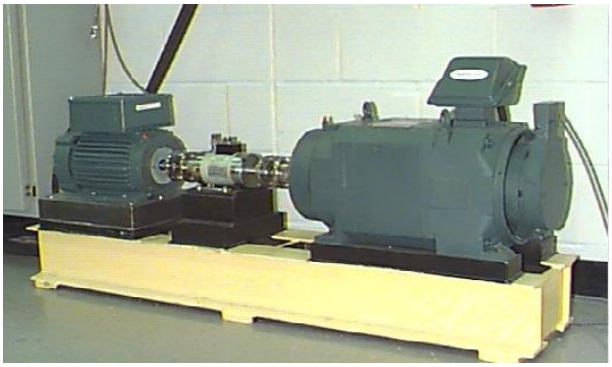

(a)

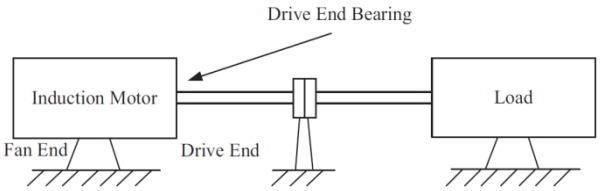

(b)

Figure 1 The experimental setup of CWRU bearing (adapted from [8]).

In this study, FNNs with the structure 4-15-7 are trained using CFS algorithms to classify the conditions of the ball bearings. These CFS algorithms were search for a combination of weights and bias parameters which results to minimum classification error for the FNNs. Two chaotic variants of SFS algorithm were used then their performances were compared to their predecessor algorithm and several well-known optimization algorithms [9].

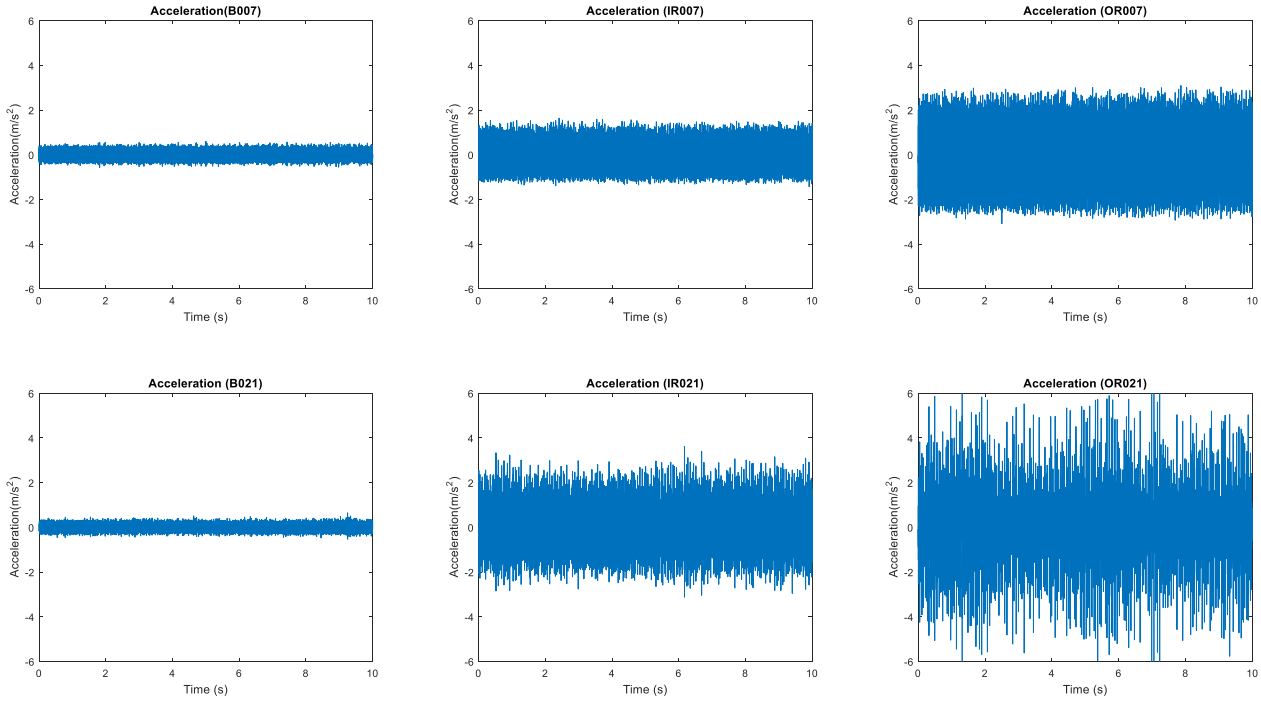

Figure 2 Acceleration data at drive end bearing with different fault types and sizes.

3. RESULTS AND DISCUSSION

Figure 3 shows the visualization of features data in 3-dimension view using principle component analysis method. All the 6 classes' faults were separable with the normal condition (dark blue). Based on Table 1, CFS04 which is SFS with Gauss/Mouse chaotic map has the highest average accuracy, 85.2833% with the standard deviation of 2.4415%. CFS04 outperformed SFS with Chebyshev chaotic map (CFS01) and its standard SFS algorithms, standard particle swarm optimization (PSO), gravitational search algorithm (GSA) and their hybrid variant (PSO-GSA) algorithms in term of average classification accuracy. However, CFS01 yield better results in term of the best and worst accuracy achieved.

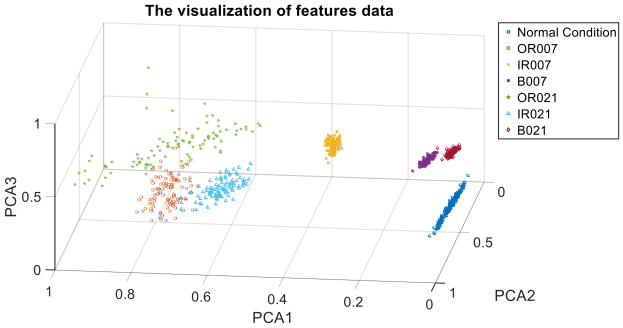

Figure 3 The visualization of features data.

4. CONCLUSION

In conclusion, two new chaotic variants of SFS algorithm were applied to train FNNs for fault diagnosis of ball bearing. SFS algorithm with Gauss/mouse chaotic map (CFS04) show superiority performance in classification rate over the other algorithms. In the future, the proposed approach can be compared with other pattern recognition methods such as support vector machines (SVMs), multilayer perceptron (MLP) or radial basis function (RBF) neural networks and also optimization of the features selection to improve the classification accuracy.

Table 1 Comparison of diagnosis results.

Algorithm	Mean	Std. dev.	Best	Worst
PSO	39.5417	8.1526	53.7500	25.6250
GSA	22.7625	23.8759	71.3750	0
PSO-GSA	44.5667	16.8728	73.6250	12.5000
SFS	85.0167	3.1520	86.3750	73.3750
CFS01	85.0208	3.0236	**86.3750**	**73.5000**
CFS04	**85.2833**	**2.4415**	86.2500	72.5000

ACKNOWLEDGEMENT

The first author would like to express his gratitude to Ministry of Higher Education (MOHE), Malaysia and Universiti Putra Malaysia (UPM) for the PhD scholarship funding. This research was performed with financial assistance under Vot No. 9540600.

REFERENCES

[1] Randall, R. B., & Antoni, J. (2011). Rolling element bearing diagnostics—A tutorial. *Mechanical systems and signal processing*, *25*(2), 485-520.

[2] Randall, R. B. (2011). *Vibration-based condition monitoring: industrial, aerospace and automotive applications*. John Wiley & Sons.

[3] Smith, W. A., & Randall, R. B. (2015). Rolling element bearing diagnostics using the Case Western Reserve University data: A benchmark study. *Mechanical Systems and Signal Processing*, *64*, 100-131.

[4] Samanta, B., Al-Balushi, K. R., & Al-Araimi, S. A. (2006). Artificial neural networks and genetic

algorithm for bearing fault detection. *Soft Computing*, *10*(3), 264-271.

[5] Salimi, H. (2015). Stochastic fractal search: a powerful metaheuristic algorithm. *Knowledge-Based Systems*, *75*, 1-18.

[6] Case Western Reserve University bearing data center. (2018). http://csegroups.case.edu/bearingdatacenter/pages/welcome-case-western-reserve-university-bearing-data-center-website

[7] Mirjalili, S., Hashim, S. Z. M., & Sardroudi, H. M. (2012). Training feedforward neural networks using hybrid particle swarm optimization and gravitational search algorithm. *Applied Mathematics and Computation*, *218*(22), 11125-11137.

[8] Zhang, X., Qiu, D., & Chen, F. (2015). Support vector machine with parameter optimization by a novel hybrid method and its application to fault diagnosis. *Neurocomputing*, *149*, 641-651.

[9] Rahman, T. A., & Tokhi, M. O. (2016). Enhanced stochastic fractal search algorithm with chaos. In *Control and System Graduate Research Colloquium (ICSGRC), 2016 7th IEEE*, 22-27.

Vibration analysis of bearing element defects operated under hexagonal boron nitride (hBN) nanoparticles mixed with diesel oil (SAE 15W40)

V. Seathuraman[1], R. Ismail[1,2,*], N.S.R. Apandi[1]

[1)] Faculty of Mechanical Engineering, Universiti Teknikal Malaysia Melaka,
Hang Tuah Jaya, 76100 Durian Tunggal, Melaka, Malaysia.
[2)] Centre for Advanced Research on Energy, Universiti Teknikal Malaysia Melaka,
Hang Tuah Jaya, 76100 Durian Tunggal, Melaka, Malaysia.

*Corresponding e-mail: rainah@utem.edu.my

Keywords: Vibration analysis; ball bearings; hexagonal boron nitride

ABSTRACT – This paper presents the investigation on vibration analysis of bearing element defects operated under hexagonal boron nitride (hBN) nanoparticle mixed with diesel oil (SAE 15W40). Ball bearing play an important role in addressing the issue of noise and vibration generators due to imperfection of geometrical bearing component, parametric excitations, stiffness in the bearing and rotation of the lubricated contacts. Considering to this problem, the potential use of hexagonal boron nitride (hBN) as additive in SAE 15W40 diesel engine oil was studied. An experimental work was conducted on a test rig to investigate the vibration characteristic of bearing element defect and effect of concentration of hBN mixed diesel oil. The results show that 0.2% concentration of hBN nanoparticle in the lubricant functioning effectively in reducing vibrations of ball bearing in diesel engine oil.

1. INTRODUCTION

A bearing is a machine element that limit relative motion to only desired motion and reduces friction between two touching surfaces. A bearing will have three usual limits to lifetime which are abrasion, fatigue and pressure-induced welding. When surface is eroded by hard contaminants, abrasion will occur that will scrap at the bearing materials. When a material become brittle after being repeatedly loaded and released fatigue will result. Pressure-induced welding can occur when two metal pieces are pressed and combined by very high pressure into a single piece.

Therefore, lubrication needed to prevent friction, corrosion and seizure on the bearing. As the present of lubricant in the bearing will increase the performance of the machine operation and speed. To improve the performance of engine, nanoparticles are added where nanoparticle works efficiency to low friction and wear. The hBN powder can be dispersed in oil lubricant, grease, solvent and water as having a strong thermal resistance and good thermal conductor. This nano-oil also actively reduced the wear rate of materials and this shows good quantitative agreement with coefficient of friction by dispersing the nanoparticles in conventional diesel engine oil[3],[4] Thus, the purpose of this study are to investigate the vibration characteristic of bearing element defect and effect of concentration of hBN mixed diesel oil. The optimized hBN nanoparticle could reduce the coefficient of friction and increase the wear resistance as compared to conventional diesel engine.

2. METHODOLOGY

An experimental setup as shown in Figure 1 is used to determine the vibration analysis of bearing element defects operated under hexagonal boron nitride (hBN) nanoparticle mixed with diesel oil (SAE 15W40).

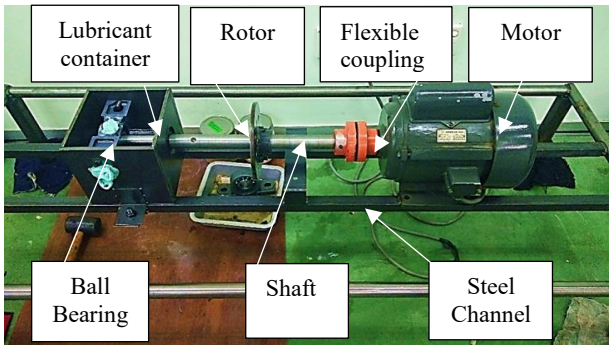

Figure 1 The experimental setup.

The main components of the experimental test rig as shown consist of motor, rotor, flexible coupling, ball bearing and lubricant container. The shaft is connected to the DC motor using the flexible coupling. Another end of shaft is also attached with a rotor at middle part and deep grove ball bearing at the end of the shaft. To reduce the vibration, all the components are installed on steel channel which are welded together. The mixture of nanoparticles in the diesel engine oil was homogenized using an ultrasonic homogenizer for 30 minutes. An accelerometer was mounted on top of the bearing housing relates to data by acquisition device DATA PHYSIC SignalCalc Analyzer connected via USB port of the PC. Different concentrations (No oil ,0%, 0.1%, 0.2% ,0.3% ,0.4% ,0.5%) of hBN nanoparticles was dispersed into SAE 15W40 diesel engine oil to determine the best concentration of hBN in reducing the vibration in ball bearing. This mixture was poured into lubricant container until the ball bearing was partially submerged by the lubricants and vibration signals were acquired.

3. RESULTS AND DISCUSSION

Based from the Figure 2 below,0.2% volume concentration of hBN shows the lowest vibration amplitude for every condition in new ball bearing with a value of 0.268m/s^2.This because, there is no defect present in the new bearing. Thus, the nanoparticles do not need to enter the surface of defected area to improve the performance. On the other hand, the highest vibration

amplitude is 0.5% volume concentration of hBN with a value of 0.289m/s^2.This is because,increasing percentage of volume concentration of hBN will cause agglomeration to occur. This agglomeration will buckle up and reduce the ability of rolling effect on the surface. Agglomeration will reduce the function of hBN nanoparticle as a friction modifier. As the friction modifiers are in micron size, it can easily enter the contact area and immediately efficient even at ambient temperature. It will change the mending effect to the rolling effect when two contact surfaces are in touch. By coating the rough friction surface, a protective film will be produced to some extent. Thus, excess present of hBN nanoparticle will increase the vibration amplitude.

From time domain approach, based on Table 1, the highest crest factor of seven condition in new bearing is no oil condition with the value of 3.56 with RMS value of 0.472 m/s^2.This is because, the present of hBN nanoparticle in the diesel engine oil can cause the formation of full film lubrication regime around the ball bearing. Thus, absent of hBN nanoparticle can cause increase in crest factor. Crest factor is a measure of a waveform that will show the ratio of peak values to the effective value. Higher crest factor will indicate high peak value in a waveform. Crest factor is the peak amplitude of the waveform divided by the Root Mean Square (RMS).0.2% volume concentration of hBN shows lowest crest factor of 3.22 as it has lowest maximum peak value of 1.39.This is because, the present of hBN nanoparticle will reduce the wear rate of materials and show good quantitative agreement with the coefficient of friction by dispersing the nanoparticle in conventional diesel engine oil.

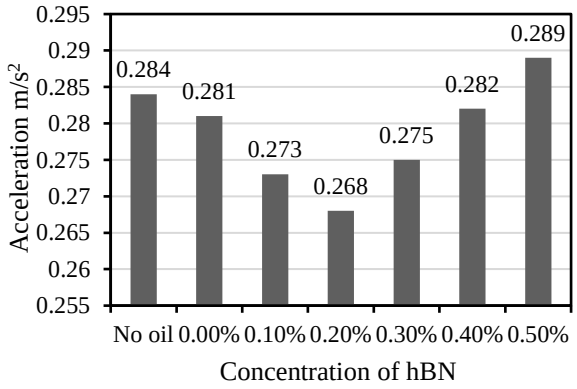

Figure 2 Graph of Acceleration vs Concentration of hBN.

Table 1 Table of RMS, Max value and Crest factor.

Condition	RMS	Max value	Crest factor
No oil	0.472	1.68	3.56
0.0%	0.453	1.58	3.49
0.1%	0.441	1.49	3.38
0.2%	0.453	1.39	3.22
0.3%	0.455	1.56	3.43
0.4%	0.458	1.58	3.46
0.5%	0.459	1.60	3.49

4. CONCLUSION

The hBN nanoparticles mixed with diesel oil can function effectively in reducing the vibration level in the new ball bearing to decrease the emission and better fuel efficiency. It can be concluded that the hBN with 0.2% of concentration gives the lower value of acceleration compared to conventional diesel engine oil for new bearing condition.

ACKNOWLEDGMENT

The authors gratefully acknowledge the Green Tribology and Engine Performances (G-TriboE) research group of Centre for Advanced Research on Energy (CARe), the financial support from Universiti Teknikal Malaysia Melaka and the ministry of Education, Malaysia under Short Term Research Grant, Grant no. RAGS/1/2014/TK01/FKM/B00066.

REFERENCES

[1] Apandi, N. S. R., Ismail, R., Abdollah, M. F. B., & Ramlan, R. (2016). Vibration characteristic on ball bearing operated with hexagonal boron nitride (hbn) nanoparticle mixed with diesel engine oil. *Proceedings of 4th Malaysia-Japan Tribology Symposium,* 25-26.

[2] Lee, J., Cho, S., Hwang, Y., Lee, C., & Kim, S. H. (2007). Enhancement of lubrication properties of nano-oil by controlling the amount of fullerene nanoparticle additives. *Tribology Letters*, *28*(2), 203-208.

[3] Jiao, D., Zheng, S., Wang, Y., Guan, R., & Cao, B. (2011). The tribology properties of alumina/silica composite nanoparticles as lubricant additives. *Applied Surface Science*, *257*(13), 5720-5725.

[4] Ilie, F., & Covaliu, C. (2016). Tribological properties of the lubricant containing titanium dioxide nanoparticles as an additive. *Lubricants*, *4*(2), 12, 1-13.

Point-to-point positioning control of a 2-DOF robotic finger for rehabilitation application

Mohamad Adzeem Mohamad Yuden[1], Mariam Md Ghazaly[1,*], Irma Wani Jamaludin[1], Aliza Che Amran[2], Zulkeflee Abdullah[3], Chin Kiat Yeo[1]

[1)] Centre for Robotics and Industrial Automation (CeRIA), Faculty of Electrical Engineering, Universiti Teknikal Malaysia Melaka, Hang Tuah Jaya, 76100 Durian Tunggal, Melaka, Malaysia.
[2)] Faculty of Engineering Technology, Universiti Teknikal Malaysia Melaka, Hang Tuah Jaya, 76100 Durian Tunggal, Melaka, Malaysia.
[3)] Faculty of Manufacturing Engineering, Universiti Teknikal Malaysia Melaka, Hang Tuah Jaya, 76100 Durian Tunggal, Melaka, Malaysia.

[*]Corresponding e-mail: mariam@utem.edu.my

Keywords: Point-to-point positioning; robotic finger; PID controller

ABSTRACT – This paper investigates the Point-to-Point (PTP) positioning control of 2 degrees of freedom (2-DOF) robotic finger mechanism for achieving high position grasping as initial research towards developing a multi-fingered robotic hand system. In this study, two different control strategies namely (i) Proportional Integral Derivative (PID) controller and (ii) Linear Quadratic Regulator (LQR) controller were chosen to be compared in experimental works. The results showed that the PID controller has higher level of adaptability for the PTP control with improvement in both response time by 97.8 % (0.079 s) and steady-state error by 98.9 % (0.02 °).

1. INTRODUCTION

In the past several decades, prosthetic hands have been developed by Zecca et al., Naidu et al. and Zhang et al. [1-3], but imitating the human hand in all its various functions, weight, visibility and appearance is still a challenging task reported by Zecca et al. [1]. Robotic hand is a device intended to be used for the rehabilitation of post-stroke patients. In general, robotic hand system requires high performance motion controller to control precisely the movement of the robotic fingers. In this case, a robust controller which offers simple design, produces fast response and excellent accuracy is desired, especially in rehabilitation application. There are many control algorithms have been proposed to control the motion of robotic hands. For example, the classical approach involves the design and implementation of PID controller. PID controller was widely implemented due to their simple structure and easy to design stated by Shauri et al. [4]. Besides that, an optimal control method such as LQR controller which takes into account the control input and states of the dynamic system offers simple design work and excellent possible performance with a multi-output system that applies the state-space method to analyze the system proved by Pavankumar et al. [5].

2. DESIGN OPTIMIZATION AND EXPERIMENTAL SETUP

In this paper, finite element analysis (FEA) technique is applied to analyze the developed robotic hand structure design via Solidworks software. Two types of FEA were evaluated; i.e. deformation test and stress test. The part labelled with A, B, C and D are the parts that force applied to the robotic hand structure for the FEA study. From FEA analysis, the total force that can be applied to the robotic hand is 50 N. The application of this force denotes the robotic hand during object manipulation. Table 1 shows the optimization parameter designs for the robotic hand system.

Table 1 Parameter designs of the robotic hand.

Parameter	Size ($l_x w_x h$)	Mass
Fingertip	$25_x 18_x 61$ mm	0.0110 kg
Finger link	$25_x 18_x 72$ mm	0.0150 kg
Thumb link	$25_x 25_x 67$ mm	0.0490 kg
Palm	$100_x 20_x 124$ mm	0.0520 kg
Total mass	-	0.4444 kg

In this study, the developed robotic hand design consists of three fingers and a thumb to cut the cost and ensure that it has sufficient flexibility for the operation purpose. Each finger has two links and 2-DOF, while thumb has three links and 3-DOF to allow adduction and abduction movement. Each joint of finger is actuated by a DC micro motor, planetary gearhead, bevel gear and optical encoder so that the developed robotic hand is small and light. The experimental setup of the developed robotic hand is shown in Figure 1.

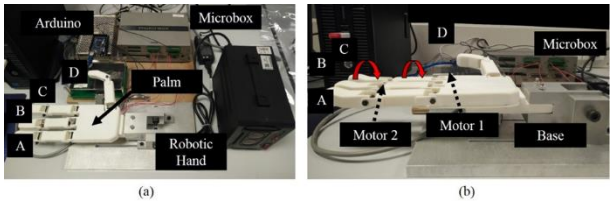

Figure 1 Experimental setup for the robotic hand.

3. RESULTS AND DISCUSSION

3.1 PID and LQR controller design procedures

In this paper, PID controller is designed using Ziegler-Nichols tuning method. The obtained ultimate gain value, K_u is 54.6 and period of oscillation, P_u is 0.015. These values are substituted into the Ziegler-Nichols Equation as shown in Equation (1) and the approximated parameters are obtained. Figure 2 shows

the block diagram of PID controller used in this study.

$$G_{PID}(s) = K_p + \frac{K_i}{s} + K_d s \quad (1)$$

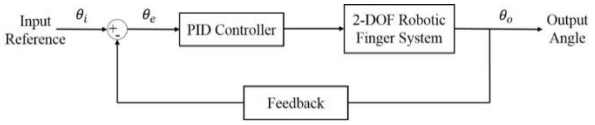

Figure 2 The block diagram of PID controller.

Meanwhile, LQR controller acquires an optimal control input by solving the Algebraic Riccati Equation. The objective of LQR controller design is to determine the state-feedback control vector, K_{LQR} that would provide the control vector, *u(t)*. The linear state feedback control law is expressed in Equation (2), which is found by minimizing a quadratic cost function shown in Equation (3). Then, the Algebraic Riccati Equation produces the Riccati solution, *P* expressed in Equation (4). Figure 3 shows the block diagram of LQR controller in this study.

$$u(t) = -K_{LQR}x(t) = -R^{-1}B^T Px(t) \quad (2)$$

$$J = \int_0^\infty [x^T(t)Qx(t) + u^T(t)Ru(t)]dt \quad (3)$$

$$A^T P + AP - PBR^{-1}B^T P + Q = 0 \quad (4)$$

Where *J* is performance index, *Q* is diagonal matrix and *R* is weight factor.

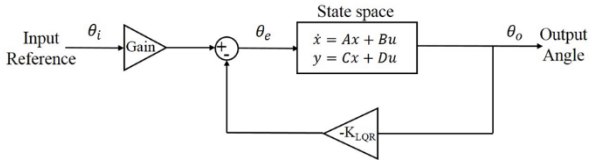

Figure 3 The block diagram of LQR controller.

3.2 Point-to-point controller performances

Experimental results show that there are significant differences between the results of uncompensated system with the PID and LQR controller. Table 2 and Figure 4 shows the performances of uncompensated, PID and LQR controller at angle of 15 °. From the results, the LQR controller presented higher steady-state error in comparison with PID controller. Real experiments show that PID controller has a faster reaction respect to the LQR controller. The closed-loop step response also compared the error and settling time with (0.02 °, 0.079 s) for PID controller and (0.02 °, 0.091 s) for LQR controller respectively. The PID controller demonstrated improvements in both response time by 97.8 % (0.079 s) and steady-state error by 98.9 % (0.02 °) over the uncompensated closed-loop system in a series of experimental step response tests.

Table 2 Performances of proposed controllers.

Performance index	Controller		
	Uncompen-sated	PID	LQR
Settling time, T_s (s)	3.584	0.079	0.091
Steady-state error, *SSE* (°)	1.982	0.02	0.02

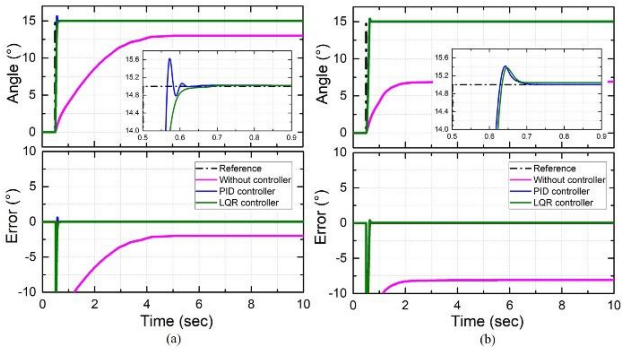

Figure 4 Experimental step response of uncompensated, PID and LQR controller for (a) Motor 1 and (b) Motor 2

4. CONCLUSION

In conclusion, the results suggested that the precision positioning PTP control of the 2-DOF robotic finger mechanism can be satisfactorily controlled via PID control approach. The PID controller demonstrated improvements in both response time by 97.8 % (0.079 s) and steady-state error by 98.9 % (0.02 °) over the uncompensated closed-loop system in a series of experimental step response tests. In this PTP, test, the PID controller has proved to be the best controller compared to LQR controller as the transient response and steady-state error is minimum in this case.

ACKNOWLEDGEMENT

This research is supported by Universiti Teknikal Malaysia Melaka grant no. JURNAL/2018/FKE/Q00006, Center for Robotics and Industrial Automation (CeRIA) and Center for Research and Innovation Management (CRIM).

REFERENCES

[1] Zecca, M., Micera, S., Carrozza, M. C., & Dario, P. (2002). Control of multifunctional prosthetic hands by processing the electromyographic signal. *Critical Reviews™ in Biomedical Engineering*, *30*(4-6). 2291-2308.

[2] Naidu, D. S., Chen, C. H., Perez, A., & Schoen, M. P. (2008, August). Control strategies for smart prosthetic hand technology: An overview. *Engineering in Medicine and Biology Society, 2008. EMBS 2008,* 4314-4317.

[3] Zhang, T., Wang, X. Q., Jiang, L., Wu, X., Feng, W., Zhou, D., & Liu, H. (2016). Biomechatronic design and control of an anthropomorphic artificial hand for prosthetic applications. *Robotica, 34*(10), 2291-2308.

[4] Shauri, R. L. A., Salleh, N. M., & Hadi, A. K. A. (2014, November). PID position control of 7-DOF three-fingered robotic hand for grasping task. *Control System, Computing and Engineering (ICCSCE),* 70-74.

[5] Pavankumar, S., Krishnaveni, S., Venugopal, Y. B., & Babu, Y. K. (2010, November). A neuro-fuzzy based speed control of separately excited DC motor. *Computational Intelligence and Communication Networks (CICN),* 93-98.

The control of an upper limb exoskeleton system for passive stroke rehabilitation: An active force control approach

A.P.P. Abdul Majeed[1,*], Z. Taha[1], M.A. Abdullah[1,2], I.M. Khairuddin[1,2], M.A. Zakaria[1]

[1)] Innovative Manufacturing, Mechatronics and Sports (iMAMS) Laboratory, Universiti Malaysia Pahang, 26600 Pekan, Pahang, Malaysia.
[2)] Department of Mechatronics Engineering, International Islamic University Malaysia, Jalan Gombak, 53100 Kuala Lumpur, Malaysia.

[*]Corresponding e-mail: anwarmajeed@imamslab.com

Keywords: Rehabilitation; active force control; artificial intelligence

ABSTRACT – This paper examines the efficacy of a robust class control scheme namely active force control (AFC) on a two degrees of freedom upper limb exoskeleton system in performing typical rehabilitation trajectory on the shoulder and elbow joints. The dynamics of the system was attained via the Lagrangian principle. The ability of the Proportional-Derivative AFC (PDAFC) architecture optimized by means of fuzzy logic (FL) and artificial neural network (ANN) against classical PD in mitigating constant disturbance effect on the aforesaid joints were also evaluated. It was demonstrated from the simulation investigation that the PDANNAFC scheme triumphs against other schemes evaluated.

1. INTRODUCTION

Approximately 15 million people around the globe suffer from stroke annually. Stroke is a neurological disorder that is caused either by an interruption of blood flow to the brain or the bleeding of the brain. Stroke survivors are often left with complete or partial paralysis that affects their activities of daily living (ADL). Nonetheless, continuous passive motion activities have been reported to allow the survivors to regain their mobility [1,2]. The employment of robotics has been seen as a potential solution towards mitigating the drawbacks of conventional rehabilitation therapy [1-3].

AFC is a robust disturbance rejection controller that was initially proposed by Hewitt and Burdess [4] in the early eighties. This scheme has been demonstrated to be satisfactory with regards to its disturbance rejection ability in both simulation and experimental works on a number of different applications [3-6]. However, it is worth to note that the efficacy of the control scheme relies upon the appropriate estimation of the estimated inertial parameter, IN. Mailah and co-researchers [6,7] have employed different intelligent algorithms in estimating the aforesaid parameter.

The aim of the present study is to investigate the effectiveness of AFC scheme in mitigating disturbance effect that is non-trivial for rehabilitation application, notably owing to the unique anthropometric properties of different individuals. Fuzzy logic (FL) and artificial neural networks (ANN) is utilised in the ascertainment of the IN parameter in the study. The ability of the PDFLAFC, PDANNAFC and the classical PD scheme in performing a joint based trajectory tacking that mimics the flexion and extension therapy against constant disturbance of 30 N.m. at a speed of 0.375 rad/s on both the shoulder and elbow joints [8].

2. METHODOLOGY

The plant of the two degrees of freedom exoskeleton system examined is derived from the Euler-Lagrange formulation restricted to the sagittal plane. For the sake of brevity, the readers are referred to [9] for the detailed derivation as well as the numerical values of the relevant parameters considered in the present study. The heuristically attained PD gains for both the shoulder and elbow joints are 1000 and 90, respectively. The predefined trajectories selected is the movement of the limbs from 0° to 90° for a period of 45 seconds that complements a typical rehabilitation activity.

FL as well as ANN were utilised in acquiring the IN parameter in the present investigation. The Mamdani fuzzy inference system with three membership functions were found to be adequate in representing the evaluated system. Equation (1) is used to determine the IN parameter.

$$IN_i = IN_{\min,i} + x_i(IN_{\max,i} - IN_{\min,i}) \quad (1)$$

Where, the subscript i denotes the joints. The constant, x is varied between 0 to 1 by means of fuzzy logic. The upper and lower bounds i.e. IN_{max} and IN_{min} are determined by heuristic means to be $0.0001 \leq IN_1 \leq 0.02$ kg.m$_2$ and $0.0001 \leq IN_2 \leq 0.005$ kg.m$_2$, respectively. The joint angles, θ_1 and θ_2 are used as the crisp input, whilst x_1 and x_2 are used as the crisp output for the fuzzification process. The fuzzy rules developed are as follows, whilst Table 1 provides the linguistic values as well as its numerical range:

a) If θ_1 is S, then x_1 is XS
b) If θ_1 is M, then x_1 is XM
c) If θ_1 is B, then x_1 is XB
d) If θ_2 is S, then x_2 is XS
e) If θ_2 is M, then x_2 is XM
f) If θ_2 is B, then x_2 is XB

A single hidden layer ANN model with a network topology of 1-10-1 was utilised in the study. The activation function employed is the logsig activation function trained with the Levenberg-Marquardt training algorithm. The input of the ANN models is θ_1 and θ_2 whilst the output of the models is, x_1 and x_2, respectively that is in accordance to Equation (1). The 70:15:15 ratio is employed for the training, testing and validation of the

models developed on a dataset of 241 points for both input and output data. The trajectory performance of the evaluated controllers is the root-mean-square-error (RMSE).

Table 1 The linguistic values and numerical range.

Linguistic Value	Numerical Range
Small (S)	0° to 22.5°
Medium (M)	22.5° to 67.5°
Big (B)	67.5° to 90°
Small (XS)	0 to 0.25
Medium (XM)	0.25 to 0.75
Big (XB)	0.75 to 1

3. RESULTS AND DISCUSSION

Figure 1 that depicts the tracking performance of evaluated controllers. It could be seen that PDAFC schemes are more superior in comparison to the classical PD scheme in mitigating the constant disturbance injected to both the shoulder and elbow joints. Moreover, it could be seen that the ANN based AFC scheme is slightly better in comparison to the FL based AFC scheme.

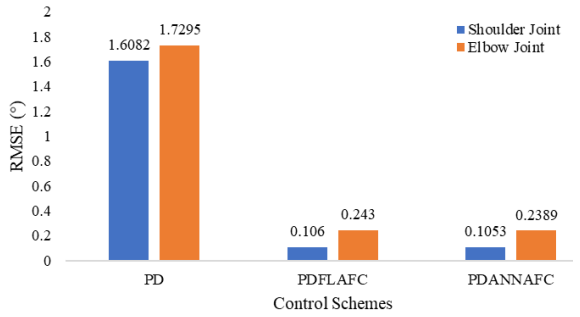

Figure 1 Tracking error performance.

The reduction of the RMSE provided by the PDANNAFC scheme against the classical PD is approximately 93 % and 86 % for the shoulder and elbow joints, respectively. This observation further suggests that the trajectory performance of the system is not compromised even in the event that disturbance is applied to the system that simulates the effect of a stroke patient upper-limb weight on the system.

4. CONCLUSION

It is apparent from the present investigation that the AFC scheme is able to mitigate the disturbance injected to the system. The PDANNAFC scheme appears to be better against the other control schemes tested, suggesting its potential employability for exoskeleton applications. Future study will explore the efficacy of the AFC scheme in real-time hardware experimentation.

REFERENCES

[1] Lo, H. S., & Xie, S. Q. (2012). Exoskeleton robots for upper-limb rehabilitation: State of the art and future prospects. *Medical Engineering and Physics*, *34*(3), 261-268.

[2] Taha, Z., Majeed, A. P. P. A., Abdullah, M. A., Khairuddin, I. M., Zakaria, M. A., & Hassan, M. H. A. (2017). The identification and control of an upper extremity exoskeleton for motor recovery *Proceedings of Mechanical Engineering Research Day*, *2017*, 483–484.

[3] Taha, Z., Majeed, A. P. A., Abidin, A. F. Z., Ali, M. A. H., Khairuddin, I. M., Deboucha, A., & Tze, M. Y. W. P. (2017). A hybrid active force control of a lower limb exoskeleton for gait rehabilitation. *Biomedical Engineering/ Biomedizinische Technik*.

[4] Hewit, J. R., & Burdess, J. S. (1981). Fast dynamic decoupled control for robotics, using active force control. *Mechanism and Machine Theory*, *16*(5), 535-542.

[5] Burdess, J. S., & Hewit, J. R. (1986). An active method for the control of mechanical systems in the presence of unmeasurable forcing. *Mechanism and Machine Theory*, *21*(5), 393-400.

[6] Priyandoko, G., Mailah, M., & Jamaluddin, H. (2009). Vehicle active suspension system using skyhook adaptive neuro active force control. *Mechanical systems and signal processing*, *23*(3), 855-868.

[7] Varatharajoo, R., Wooi, C. T., & Mailah, M. (2011). Attitude pointing enhancement for combined energy and attitude control system. *Acta Astronautica*, *68*(11-12), 2025-2028.

[8] Nef, T., Mihelj, M., & Riener, R. (2007). ARMin: a robot for patient-cooperative arm therapy. *Medical & Biological Engineering & Computing*, *45*(9), 887-900.

[9] Taha, Z., Majeed, A. P. A., Tze, M. Y. W. P., Hashem, M. A., Khairuddin, I. M., & Razman, M. A. M. (2016, February). Modelling and control of an upper extremity exoskeleton for rehabilitation. *IOP Conference Series: Materials Science and Engineering, 114*(1), 1-8.

Static analysis of tunable piecewise stiffness mechanism using vertically constrained cantilever beam

Muhammad Harith Mustaffer[1], Roszaidi Ramlan[1,2,*], Mohd Nazim Abdul Rahman[1,2], Azma Putra[1,2]

[1)] Faculty of Mechanical Engineering, Universiti Teknikal Malaysia Melaka,
Hang Tuah Jaya, 76100 Durian Tunggal, Melaka, Malaysia.
[2)] Centre for Advanced Research on Energy, Universiti Teknikal Malaysia Melaka,
Hang Tuah Jaya, 76100 Durian Tunggal, Melaka, Malaysia.

[*]Corresponding e-mail: roszaidi@utem.edu.my

Keywords: Nonlinear; hardening; piecewise

ABSTRACT – This paper investigates the characteristics of a newly designed tunable piecewise stiffness mechanism to produce hardening-like stiffness effect. The hardening-like stiffness effect is proven to perform better especially when it is used as the nonlinear dynamic vibration absorber (NDVA). The mechanism is mainly made of a cantilever beam constrained by two limit blocks which are adjustable in both horizontal and vertical direction. Analytical and numerical studies were conducted to obtain the force-deflection characteristics. The results were then validated using quasi-static measurement. Analytical, numerical and experimental results compared well and proved the ability of the mechanism to produce wide range piecewise stiffness characteristics.

1. INTRODUCTION

Vibration control measure can be mainly classified into passive vibration, semi-active vibration, and active vibration control. Among these, passive vibration control using dynamic vibration absorber (DVA) has been one of the effective methods to control the structural vibration in buildings, bridges and automotive components. The fundamental concept of the linear DVA is to design the absorber with a natural frequency which matches the resonance frequency of the vibrating structure. However, such tuning method is only effective to suppress the vibration in a narrow frequency range and the vibration of the structure will be amplified outside the tuned frequency range[1-2]. This paper focuses on designing a tuneable piecewise stiffness mechanism which is able to operate in a wide frequency range similar to commonly used nonlinear hardening stiffness. This is done by constraining a cantilever beam between the two limit blocks with adjustable horizontal and vertical distances. The force (F) and deflection (y) characteristics of the mechanism are investigated analytically and numerically. The results are validated experimentally using quasi-static measurement.

2. METHODOLOGY

2.1 Analytical study

Initially the expression for the force-deflection shown in Eq. (1) was derived using the Double Integration method [3] based on the schematic shown in Figure 1. In this case, the stiffness is broken up into two. The first is when the beam does not contact the limit blocks and the second is when it touches the limit blocks and move under constrained motion.

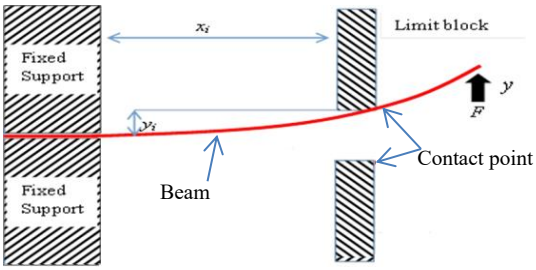

Figure 1 Schematic of piecewise stiffness mechanism.

$$F(y)=\begin{cases}\dfrac{3EIy}{L^3} \\ -\dfrac{6(-2yx_i+3Ly-x_iy_i)EI}{x(4L^3-9xL^2+6x^2L-x^3)}\end{cases} \quad (1)$$

2.2 Numerical study

Numerical study on the static property of the mechanism was studied using ANSYS software as shown in Figure 2. The specifications of the beam are presented in Table 1. The results were compared to the analytical results obtained previously.

Table 1 Beam specifications.

Material	Stainless steel
Bending Rigidity, *EI*	0.13 Nm^2
Length, *L*	80 mm
Width, *b*	26 mm
Thickness, *t*	0.6 mm
Seismic mass	22 g
Horizontal distance (x_i)	25 mm, 35 mm, 45 mm
Vertical gap (y_i)	2 mm

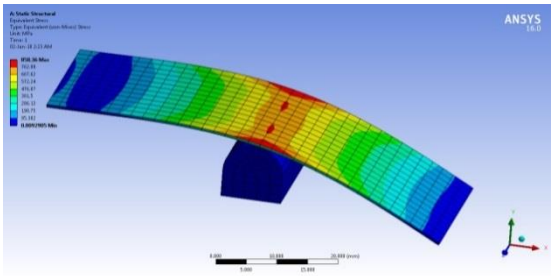

Figure 2 FEA of the piecewise stiffness mechanism.

2.4 Experimental study

Once the analytical and numerical results were validated, then mechanism was fabricated. Experimental study was conducted using quasi-static measurement technique in order to obtain the force-deflection characteristic of the mechanism under various configurations. Three horizontal distances, x_i (25 mm, 35 mm, and 45 mm) and a single vertical gap, y_i of 1 mm were investigated. The LDS V406 electrodynamic shaker was used to excite the motion at roughly 1 Hz. The restoring force was measured by Tedea Huntleigh compression load cell while the tip deflection was measured using Keyence Laser Triangulation Sensor. The brief experimental setup is shown in Figure 3. The results were then fitted to cubic polynomial in the form of $k_1 x + k_3 x^3$, where k_1 is the linear stiffness and k_3 is the nonlinear stiffness [3].

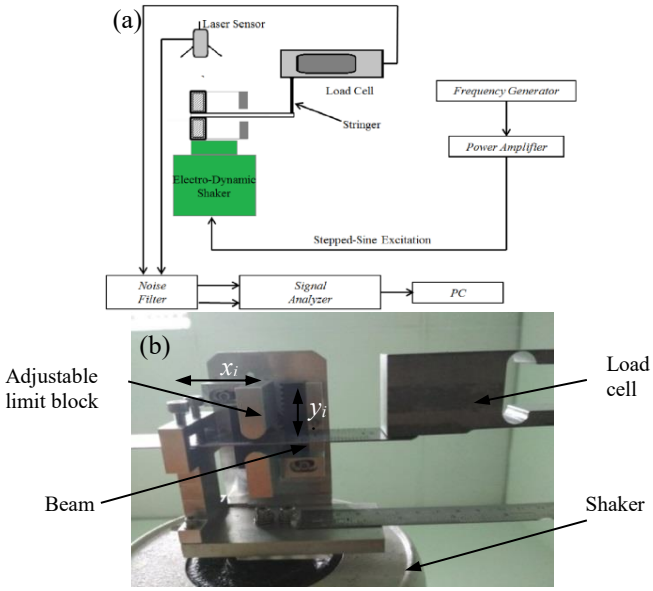

Figure 3 (a) Setup for quasi-static measurement, (b) Close-up view of fabricated mechanism.

3. RESULTS AND DISCUSSION

3.1 Analytical and numerical study

Figure 4 shows the good agreement between the analytical and numerical force-deflection results of the proposed mechanism for y_i = 2 mm with three different x_i of 25 mm, 35 mm, and 45 mm, respectively. This clearly shows the existence of the piecewise stiffness. The lower stiffness refers to the unconstrained motion while the second refers to the constrained motion. As x_i increases, the unconstrained deflection range reduces and the stiffness becomes harden even for a small tip deflection. This is due to the small amount of tip deflection required to reach the limit blocks as x_i increases [4].

3.2 Quasi-static measurement

Figure 5 shows the comparison between the analytical and experimental force-deflection results. The experimental results are fitted with cubic polynomial. This figure shows a reasonable agreement between the results. Slight deviation occurs at large deflection range which may be due to the effect of rotation between the tip of the beam and the load cell. Nonetheless, the deflection range in the good agreement region is enough to make this mechanism useful in applications such as in dynamic vibration absorption (DVA). The ability for the piecewise stiffness to behave as hardening-type stiffness may be beneficial in increasing the effective bandwidth of DVA.

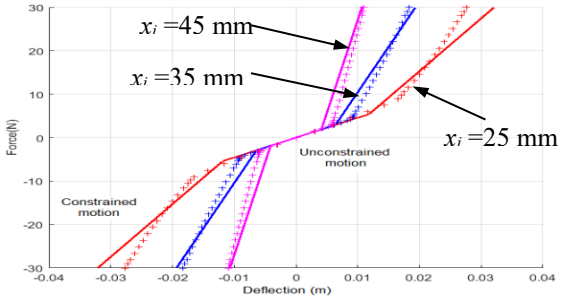

Figure 4 Analytical (-) and numerical (+) results.

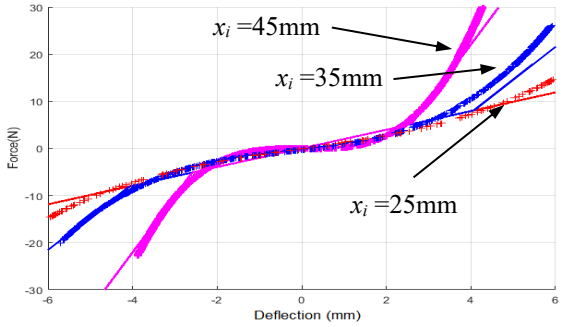

Figure 5 Experimental (+) and analytical results (-).

4. CONCLUSION

The proposed piecewise stiffness mechanism has been analyzed and tested. Most importantly, it is worth to note that this stiffness of mechanism is a piecewise version of the hardening stiffness which has been widely used in improving the bandwidth of DVAs. However, the proposed mechanism offers versatility in terms of stiffness tuning ability, which existing approaches are not able to do so.

ACKNOWLEDGEMENT

This project is supported by Ministry of Higher Education Malaysia (Grant number: FRGS/1/2016/TK03/FKM-CARe/F00318).

REFERENCES

[1] Hoffmann, D., Folkmer, B., & Manoli, Y. (2012). Comparative study of concepts for increasing the bandwidth of vibration based energy harvesters. *Proceedings of PowerMEMS, 2012*, 219-222.

[2] Ramlan, R., Brennan, M. J., Mace, B. R., & Kovacic, I. (2010). Potential benefits of a non-linear stiffness in an energy harvesting device. *Nonlinear Dynamics*, *59*(4), 545-558.

[3] Hibbeler, R. C. (2008). *Mechanics of Materials*, 7th ed. Pearson Education and South Asia Pte Ltd.

[4] Shui, X., & Wang, S. (2018). Investigation on a mechanical vibration absorber with tunable piecewise-linear stiffness. *Mechanical Systems and Signal Processing*, *100*, 330-343.

An investigation on tool wear monitoring using MFC and PVDF sensors via I-kaz™ statistical signal analysis

Muhamad Arif Fadli Ahmad[1], Mohd. Zaki Nuawi[1,*], Jaharah A. Ghani[1], Shahrum Abdullah[1], Mohd Irman Ramli[1,2]

[1)] Department of Mechanical and Materials Engineering, Faculty of Engineering and Built Environment, Universiti Kebangsaan Malaysia, 43600 UKM Bangi, Selangor, Malaysia.
[2)] Faculty of Engineering Technology, Universiti Teknikal Malaysia Melaka, Hang Tuah Jaya, 76100 Durian Tunggal, Melaka, Malaysia.

[*]Corresponding e-mail: mzn@ukm.edu.my

Keywords: Tool wear monitoring; MFC; PVDF; Statistical signal analysis; I-kaz; Vibration signal

ABSTRACT – This paper investigates the performance of low-cost MFC and PVDF sensors in tool wear monitoring by utilising I-kaz™ statistical signal analysis method. The sensors were mounted on a tool holder inside CNC turning machine. The experiment was done by turning a workpiece in a dry condition and stopped once the cutting tool reached 0.3 mm of flank wear. The sensor signals were recorded, extracted and analysed. The result indicated that both sensors responded well with the wear progression. However, MFC performed better by providing a higher correlation.

1. INTRODUCTION

There is a real need to devise a reliable and low cost tool wear monitoring system as tool wear is the most undesirable occurrence that continues to plague the manufacturing industries, affecting quality of finished products [1]. Two methods of tool wear monitoring are generally utilised, which are direct and indirect. Direct monitoring related to the optical approach while indirect involved the use of suitable sensors to acquire the signal data. Wear could be empirically determined by analysing the force, sound, vibration, acoustic emission and temperature [2]. Macro fibre composite (MFC), lead zirconate titanate (PZT) and polyvinyldene fluoride film (PVDF) are piezoelectric element materials that are widely used as vibration sensors and energy density harvesters as well as low power consumption actuators [3]. Random signals such as in machining are commonly quantified by standard deviation, variance, skewness, kurtosis and rms statistical features, but there were certain limitations emerged as found by past researchers [4]. Thus, an alternative way known as Integrated Kurtosis-based Algorithm for Z-notch filter (I-kaz™) pioneered by Nuawi et al. [4] was built and served as a supplement to provide a better and reliable signal feature.

2. METHODOLOGY

The schematic illustration of the research is depicted in Figure 1. The experiment was carried out by turning 40 HRC of hardened AISI 4340 round bar using Cholchester Tornado T8 CNC turning machine in a dry condition where Sumitomo AC2000 was chosen as a cutting tool. The machining parameter being used is shown in Table 1. MFC used was M2814-P2 with 28 x 14 mm active size whereas PVDF was LDT1-028K with 30 x 12.16 mm (length x width). Both are anisotropic type of materials. They were mounted at the top and bottom of a tool holder perpendicular with the cutting force direction. Vibration signals from sensors were recorded and flank wear was measured using microscope for every machining run. They stopped once the tool reached 0.3 mm of average wear according to ISO 3685 standard. Signal data from both sensors were charge amplified using Piezo Film Lab Amplifier power modules with 10 nF of feedback capacitance before being acquired with NI 9234 data acquisition modules and computer. The sampling frequency and rate was set to 25.6 kHz and 25.6 kS/s with 24-bit resolution.

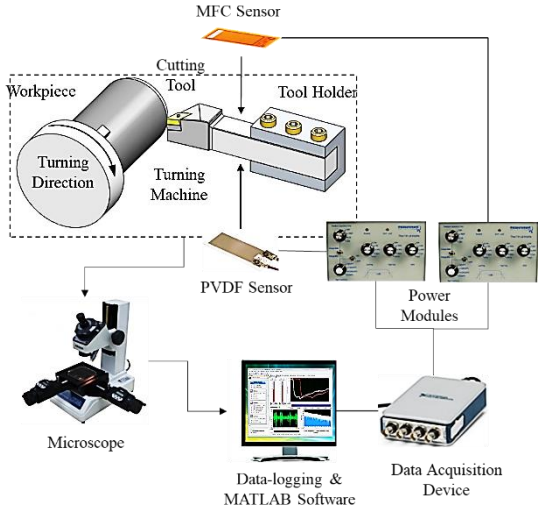

Figure 1 Schematic illustration of the research study.

Table 1 Machining parameter.

Set	Cutting speed (m/min)	Depth of cut (mm)	Feed rate (mm/rev)
1	200	0.12	0.25
2	250	0.12	0.25
3	300	0.12	0.25

The acquired signals were analysed using I-kaz™ alternative statistical method. For n-number of data, I-kaz coefficient, Z^{∞} was derived as in Equation (1).

$$Z^{\infty} = \frac{1}{n}\sqrt{K_L s_L^4 + K_H s_H^4 + K_V s_V^4} \quad (1)$$

Where K_L, K_H, K_V and s_L, s_H, s_V are kurtosis and standard deviation for low, high, and very high frequency range respectively.

3. RESULTS AND DISCUSSION

3.1 Wear progression towards recorded signal amplitude

Figure 2 shows an example of time domain for initial and final stage of wear progression for MFC in set 3. The machining signal data were comprising of random stationary signals with kurtosis value around 3. The amplitude signals were roughly observed to be slightly increased when wear rose from initial to final. The same observation went for PVDF.

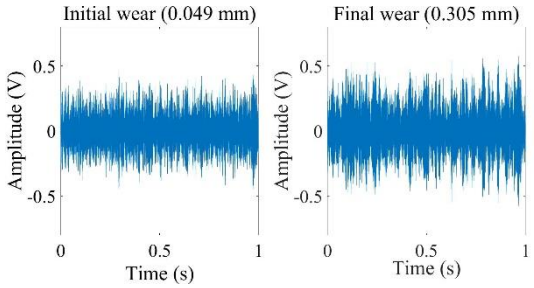

Figure 2 Time domain of machining signal on initial and final wear measurement of MFC from set 3.

3.2 Correlation between I-kaz coefficients with wear progression

The recorded signals were statistically analysed using I-kaz^{TM} signal feature as in Equation (1). Table 2 shows Z^{∞} and wear for set 3. They were then correlated and tabulated in graph using simple regression analysis. The graphs are presented in Figure 3 (MFC) and Figure 4 (PVDF) for all sets. A linear equation model was selected as the best fit for all sets. The correlation of determination, R^2 produced by the model is tabulated in Table 3. The result indicated that the average R^2 of MFC and PVDF were 0.7708 and 0.6843 respectively. As asserted by Jemielniak et al. [5], R^2 above 0.6 was considered a good signal feature and wear correlation. Thus, both sensors performed well and produced an acceptable R^2. However, MFC performed better with higher R^2 mainly because PVDF happened to be more affected by disturbance and its lack of electro-mechanical coupling efficiency making it less sensitive [6].

Table 2 I-kaz coefficient with wear progression for set 3.

Wear (mm)	Z^{∞} (MFC)	Z^{∞} (PVDF)
0.049	9.68E-07	5.24E-09
0.096	1.05E-06	5.68E-09
0.151	1.37E-06	5.77E-09
0.189	1.35E-06	5.62E-09
0.225	1.52E-06	6.46E-09
0.264	1.73E-06	6.78E-09
0.305	1.63E-06	6.13E-09

Table 3 Correlation of determination, R^2 for all experimental sets.

Sensor	Set 1	Set 2	Set 3	Average
MFC	0.6648	0.7300	0.9177	0.7708
PVDF	0.9103	0.5010	0.6416	0.6843

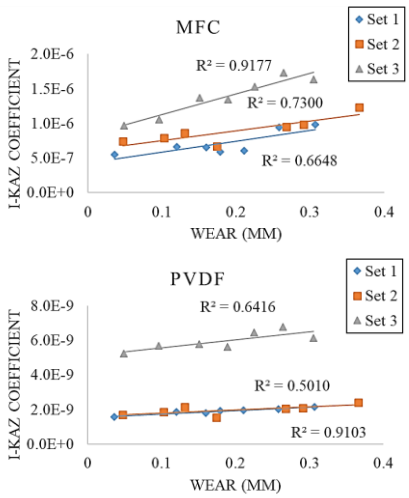

Figure 3 Graph of correlation between I-kaz coefficient with wear progression for MFC and PVDF.

4. CONCLUSION

In conclusion, tool wear monitoring by utilising low-cost MFC and PVDF sensors using I-kaz^{TM} statistical signal feature have been successfully developed. Both sensors showed acceptable result, however MFC providing better correlation than PVDF. The correlation indicated a larger R^2 on MFC with an average of 0.7708, whereas it was 0.6843 for PVDF. This new finding would encourage further studies on the MFC and PVDF sensors in tool wear prediction system.

ACKNOWLEDGEMENT

The authors wish to express their gratitude to Universiti Kebangsaan Malaysia (UKM) and the Ministry of Higher Education of Malaysia for providing the financial support.

REFERENCES

[1] Snr, D. E. D. (2000). Sensor signals for tool-wear monitoring in metal cutting operations - A review of methods. *International Journal of Machine Tools and Manufacture*, *40*(8), 1073-1098.

[2] Bhuiyan, M. S. H., & Choudhury, I. A. (2014). Review of Sensor Applications in Tool Condition Monitoring in Machining. *Comp. Mater. Process*, *13*, 539-569.

[3] Khan, A., Abas, Z., Kim, H. S., & Oh, I. K. (2016). Piezoelectric thin films: an integrated review of transducers and energy harvesting. *Smart Materials and Structures*, *25*(5), 1-16.

[4] Nuawi, M. Z., Nor, M. J. M., Jamaludin, N., Abdullah, S., Lamin, F., & Nizwan, C. K. E. (2008). Development of integrated kurtosis-based algorithm for z-filter technique. *Journal of Applied Sciences*, *8*(8), 1541-1547.

[5] Jemielniak, K., Urbański, T., Kossakowska, J., & Bombiński, S. (2012). Tool condition monitoring based on numerous signal features. *The International Journal of Advanced Manufacturing Technology*, *59*(1-4), 73-81.

[6] Sohn, J. W., Jeon, J., & Choi, S. B. (2013). An investigation on dynamic signals of MFC and PVDF sensors: experimental work. *Advances in Mechanical Engineering*, *5*, 1-9.

Parametric study on performance of an inhomogeneous MPP absorber

Ali I. Mosa[1,3,*], A. Putra[1,2], R. Ramlan[1,2], Al-Ameri Esraa[1], Z. Halim[1,2]

[1)] Faculty of Mechanical Engineering, Universiti Teknikal Malaysia Melaka,
Hang Tuah Jaya, 76100 Durian Tunggal, Melaka, Malaysia.
[2)] Centre for Advanced Research on Energy, Universiti Teknikal Malaysia Melaka,
Hang Tuah Jaya, 76100 Durian Tunggal, Melaka, Malaysia.
[3)] Mechanical Engineering Department, Collage of Engineering, University of Baghdad, Jadriyah - Baghdad, Iraq.

[*]Corresponding e-mail: azma.putra@utem.edu.my

Keywords: Sound absorption, inhomogeneous MPP, multi-cavity depth

ABSTRACT – Micro-perforated panel absorber (MPP) has been proposed as an alternative absorber to porous materials. It is made from a panel and thus it simple to be installed, long durability, clean and has attractive appearance. However, realization of broad frequency bandwidth of absorption in MPP still pose a challenging problem. Here, parametric study for an inhomogeneous MPP absorbers with multi-depth of backed air cavity is proposed. The model is based on the equivalent circuit method. The simulation shows that adjustment of the cavity depth, panel thickness, hole size and perforation ratio can improve the absorption level and extends the absorption bandwidth.

1. INTRODUCTION

Green material as sound absorbers have gained attention of researchers due to their advantages over porous absorbing materials, which are destructive to environment and human health [1]. The MPP with broader range of absorption frequency has been proposed by combining two layers of MPPs having different perforation ratios with the same backed cavity depth set in parallel and consecutively to each other [2]. Theoretical and experimental investigations for different backed cavity depths in parallel array of multiple symmetric MPPs absorbers for normal incidence wave has also been proposed [3]. In order to improve the sound absorption in the low- to mid- frequency range (100–1600 Hz) under the space constraint of about 100mm depth, combinations of parallel-arranged PPETs and porous sound absorptive material (PSAM) are investigated [4]. Although the MPPs absorber generally made of a thin panel which can limit their applications, a thick panel of inhomogeneous MPP absorber is also studied. Results showed that the bandwidth frequency of absorption for thick inhomogeneous MPPs could be two times than that of the thin panels [5]. This paper proposes mathematical model of inhomogeneous MPP arrays with multi-depth backed air cavities under normal sound incident to widen the absorption bandwidth frequency.

2. METHODOLOGY

Schematic diagram of inhomogeneous MPP absorbers (with different hole sizes and perforation ratios), with different air cavity depth for each panel is shown in Figure 1. The thickness is the same and the mathematical model based on the equivalent electrical circuit method was developed .

For n number of MPPs, the acoustic impedance of the n-th MPP at normal incidence is given by [6]

$$Z_{MPP,n} = \frac{R_n + jM_n}{\rho c} \quad (1)$$

Where ρ is the air density, c is the speed of sound, ω is the angular frequency and R and M are the specific acoustic resistance and the specific acoustic reactance, respectively which can be referred in [5].

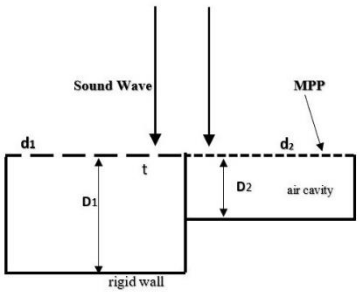

Figure 1 Inhomogeneous MPP in series arrangement.

The normalized specific acoustic impedance with air cavity depth of D is given by [6]

$$Z_{D,n} = -jcot(\omega D_n / c_o) \quad (2)$$

The total absorption coefficient of the MPP system under normal incident of sound is given by

$$\alpha = \frac{4Re(Z_{total})}{[1+Re(Z_{total})]^2+[Imag(Z_{total})]^2} \quad (3)$$

Where Z_{total} is the total system impedance.

3. RESULTS AND DISCUSSION

Figure 2 shows the effect of thickness on the inhomogeneous MPP absorber on sound absorption coefficient at frequency up to 1600 Hz. It can be observed that increment of the panel thickness widens the absorption bandwidth and improved MPP panel sound absorption performance. The improvement can be seen towards low frequency region as the thickness of the panel is increased.

Figure 3 shows the results for variation of hole size diameters with constant panel thickness. The absorption performance can be seen to be sensitive to the combination of hole size for each panel.

It can be seen that combination of the MPP panels with any size of diameter with that having 3 mm hole size

produces wider bandwidth and greater absorption, compared if combined with 1 mm hole size. Optimum hole diameter is thus important to produce good absorption.

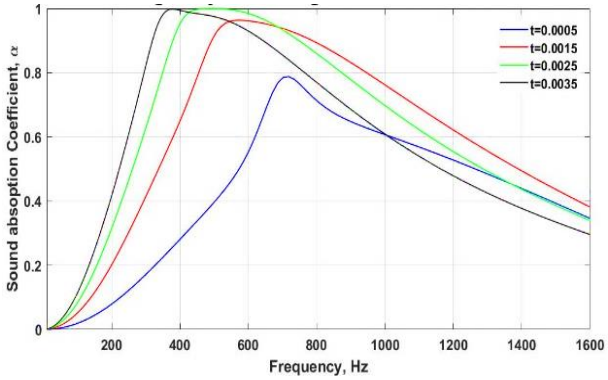

Figure 2. Effect of panel thickness (in m) on absorption coefficient of inhomogeneous MPP absorbers: D_1=0.03 m, D_2=0.075 m, d_1=0.9 mm, d_2=0.3 mm, p_1=0.6%, p_2=4%.

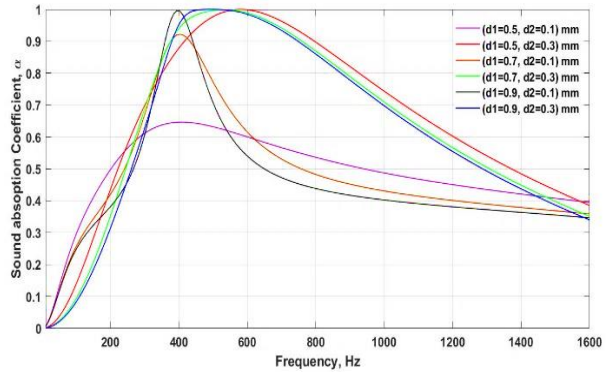

Figure 3. Effect of hole diameter on absorption coefficient of inhomogeneous MPP absorbers: D_1=0.03 m, D_2=0.075 m, p_1=0.6%, p_2=4%, t = 2.5 mm.

Figure 4 shows that the sound absorption moves to the lower frequency region with the increase of the backed cavity depth, with slightly decreasing in value of the absorption coefficient. The bandwidth of absorption depends with the combination of hole diameter.

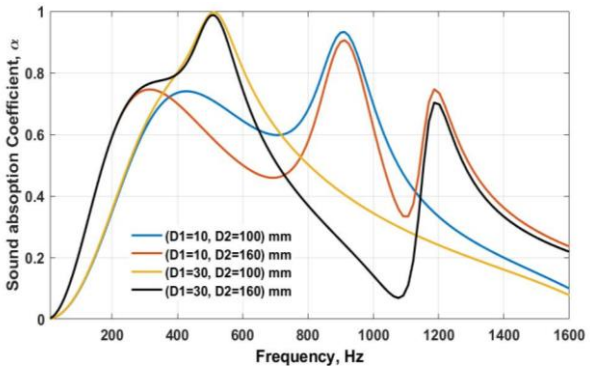

Figure 4. Effect of backed cavity depth on absorption coefficient of inhomogeneous MPP absorbers: d_1=0.9 mm, d_2=0.3 mm, p_1=0.8%, p_2=2%, t = 1.8 mm.

4. CONCLUSION

Parametric study of the inhomogeneous MPP absorber with multi-depth of backed air cavities has been proposed. It was found that adjustment of the panel thickness, variation of hole size, perforation ratio and backed cavity depth can improve the absorption performance of MPP panel by broadening the absorption bandwidth as well as increase the absorption coefficient level.

ACKNOWLEDGEMENT

Part of this project is supported by the Fundamental Research Grant Scheme from Ministry of Higher Education Malaysia.
(Grant no.: FRGS/1/2016/TK03/FTK-CARE/F00323)

REFERENCES

[1] Or, K. H., Putra, A., & Selamat, M. Z. (2016). Mathematical modeling on sound absorption of oil palm empty fruit bunch fibers. *Proceedings of Mechanical Engineering Research Day*, *2016*, 214-215.

[2] Sakagami, K., Nagayama, Y., Morimoto, M., & Yairi, M. (2009). Pilot study on wideband sound absorber obtained by combination of two different microperforated panel (MPP) absorbers. *Acoustical Science and Technology*, *30*(2), 154-156.

[3] Wang, C., & Huang, L. (2011). On the acoustic properties of parallel arrangement of multiple micro-perforated panel absorbers with different cavity depths. *The Journal of the Acoustical Society of America*, *130*(1), 208-218.

[4] Li, D., Chang, D., & Liu, B. (2017). Enhanced low-to mid-frequency sound absorption using parallel-arranged perforated plates with extended tubes and porous material. *Applied Acoustics*, *127*, 316-323.

[5] Vidal-Quist, J. C., Ortego, F., Castanera, P., & Hernández-Crespo, P. (2017). Quality control of house dust mite extracts by broad-spectrum profiling of allergen-related enzymatic activities. *Allergy*, *72*(3), 425-434.

[6] Maa, D. Y. (1987). Microperforated-panel wideband absorbers. *Noise Control Engineering Journal*, *29*, 77-84.

Effect of low frequency excitation location for crack detection in nonlinear vibro-acoustic method

Tino Hermanto[1], Ruztamreen Jenal[1,2], Abd Rahman Dullah[1,2,*], Nor Salim Muhammad[1,2], Azma Putra[1,2], Reduan Mat Dan, Ahmad Fuad Ab Ghani[1,2]

[1)] Faculty of Mechanical Engineering, Universiti Teknikal Malaysia Melaka, Hang Tuah Jaya, 76100 Durian Tunggal, Melaka, Malaysia.
[2)] Centre for Advanced Research on Energy, Universiti Teknikal Malaysia Melaka, Hang Tuah Jaya, 76100 Durian Tunggal, Melaka, Malaysia.

[*]Corresponding e-mail: abdrahman@utem.edu.my

Keywords: Non-linear vibro-acoustics; laser doppler vibrometer; vibro acoustic modulation

ABSTRACT – This paper investigates the effect of three different low frequency excitations and locations on centre cracked aluminium plate by using nonlinear vibro-acoustic method. The test rig consist of mechanical shaker and PZT transducer were used to provide simultaneous interaction between low frequency excitation and high frequency inputs. Seven excitation locations under the crack were tested. R value is used to determine the most effective frequency and excitation location. The result shows that 1st vibration mode frequency produces the significant effect on defect detection with effective location for excitations at the centre near the crack line and at the edge of plate.

1. INTRODUCTION

Vibro-acoustic Modulation (VAM) [1,2] is a test that introduces two high and low frequency signals into a specimen simultaneously. Interaction of the wave with present of non-uniformity of structure such as crack will be produce nonlinear wave interaction effect such as sidebands around the high frequency signal peaks. The intensity of the sideband around the high frequency signal will indicate the severity or size of the damage or crack [3]. Using VAM, Simondi et al. [4] successfully detected cracks in solid and metallic structure. Duffour et al. [2] addressed on averaging the amplitude of the sidebands over a wide ultrasonic frequency to eliminate the dependence of the sensitivity of VAM on ultrasonic frequency.

Current studies usually regard the ratio of the sidebands and the main peak as a damage index to indicate the presence of cracks. Hu et al. [5] found that the damage index calculated in the spectrum domain may lead to false indications about the damage severity owning the complex modulation processes.

However, the sideband intensity also may differs depending on the condition when performing the test such as on the condition of the low frequency excitation location. Therefore, this paper presents an experiment result to show the effect of low frequency excitation location in vibro-acoustic test for the crack detection with the intensity of the nonlinear wave interaction.

2. METHODOLOGY

Similar experimental set up as proposed by Hermanto et al. [6] is used to determine the modal analysis of three different vibration mode frequencies on 35 mm centre cracked aluminium plate Al-2024 (400mm x 150mm x 2mm) as shown in Figure 1.

The modal analysis found that the frequency for 1st, 2nd and 3rd vibration mode is 66Hz, 106Hz and 184Hz respectively. These frequencies were used to excite the cracked plate at each 7 locations along with low amplitude of 60 kHz high frequency signal as shown in Figure 1.

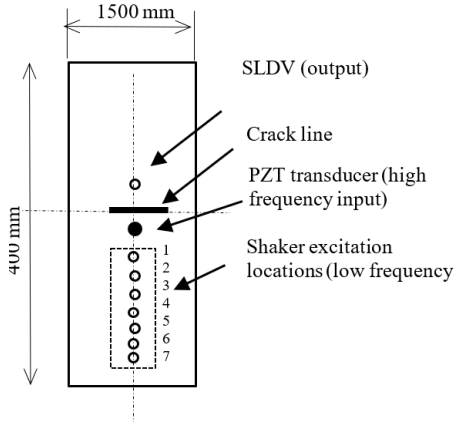

Figure 1 Schematic diagram of the excitation location on the aluminium plate.

The velocity of the plate vibration responses in time domain was measured by using scanning laser Doppler vibrometer (SLDV). Then the measured data was transformed to frequency domain by using Fast Fourier Transform (FFT).

At high frequency band, the present of sideband around 6o kHz peak was observed as shown in Figure 2.

The sideband frequency gap is equivalent to the low frequency value. Intensity of the sideband was calculated by using R value,

$$R = \frac{A_1 + A_2}{A_0} \quad (1)$$

Where, A_0 is high frequency amplitude and A_1 and A_2 are first sideband amplitudes on the left and right of the high frequency peak.

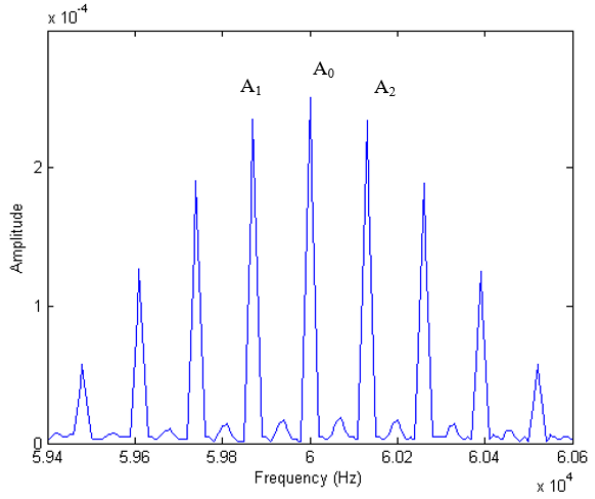

Figure 2 Power spectrum of the high frequency signal at 60 kHz.

3. RESULTS AND DISCUSSION

Figure 3 shows R values against 1st, 2nd and 3rd vibration mode frequency excitations at shaker excitation locations. The 1st vibration mode excitation shows the highest R value compared to the others vibration mode excitation with the maximum value near crack line (point 7) and at plate edge (point 1) while the minimum value is at the centre of the measured points (point 4).

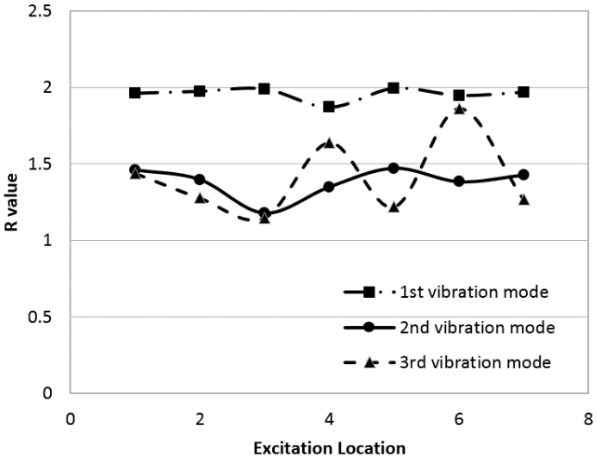

Figure 3 Graph of R value against excitation location for three vibration mode frequencies.

In the 2nd and 3rd vibration mode frequency excitations, there are no significant trending that could be related with the excitation locations. However, the R values are lower than the values from the 1st vibration mode excitation at most of the excitation locations due to low surface deflections.

4. CONCLUSIONS

The 1st vibration mode shows the highest non-linear wave interaction, it is considered as the most effective mode for fatigue crack detection. The most effective excitation locations are at centre and edge of the plate.

ACKNOWLEDGEMENT

Authors would like to acknowledge Universiti Teknikal Malaysia Melaka for the Zamalah Scheme awarded to the first author.

REFERENCES

[1] Hood, A., Samuel, P., & Pines, D. J. (2005). A vibro-acoustic methodology for the detection and characterization of spur gear tooth damage. *Annual Forum Proceedings-American Helicopter Society, 61*(2), 1268.

[2] Duffour, P., Morbidini, M., & Cawley, P. (2006). A study of the vibro-acoustic modulation technique for the detection of cracks in metals. *The Journal of the Acoustical Society of America*, *119*(3), 1463-1475.

[3] Parsons, Z., & Staszewski, W. J. (2006). Nonlinear acoustics with low-profile piezoceramic excitation for crack detection in metallic structures. *Smart Materials and Structures*, *15*(4), 1110.

[4] Simondi, M., Staszewski, W. J., & Jenal, R. B. (2009l). Structural damage detection using ultrasonic wave modulation with low-profile piezoceramic transducers. *Health Monitoring of Structural and Biological Systems, 7295,* 1-9.

[5] Hu, H. F., Staszewski, W. J., Hu, N. Q., Jenal, R. B., & Qin, G. J. (2010). Crack detection using nonlinear acoustics and piezoceramic transducers—instantaneous amplitude and frequency analysis. *Smart Materials and Structures*, *19*(6), 065017.

[6] Hermanto, T., Dullah, A. R., Jenal, R., & Muhammad, N. S. (2017). Stress determination by using out-of-plane deflection with scanning laser doppler vibrometer. *Science & Technology Research Institute for Defence, 10*(1), 51-61.